Available online at www.sciencedirect.com
SCIENCE DIRECT®
Remote Sensing of Environment 89 (2004) 510–518
Remote Sensing of Environment
www.elsevier.com/locate/rse

Combining satellite multispectral image data and a digital elevation model for mapping debris-covered glaciers

Frank Paul*, Christian Huggel, Andreas Kääb

Department of Geography, Glaciology and Geomorphodynamics Group, University of Zürich-Irchel, Winterthurerstr. 190, CH-8057 Zurich, Switzerland

Received 9 September 2003; received in revised form 10 November 2003; accepted 11 November 2003

Abstract

Automated glacier mapping from satellite multispectral image data is hampered by debris cover on glacier surfaces. Supraglacial debris exhibits the same spectral properties as lateral and terminal moraines, fluvioglacial deposits, and bedrock outside the glacier margin, and is thus not detectable by means of multispectral classification alone. Based on the observation of low slope angles for debris-covered glacier tongues, we developed a multisource method for mapping supraglacial debris. The method combines the advantages of automated multispectral classification for clean glacier ice and vegetation with slope information derived from a digital elevation model (DEM). Neighbourhood analysis and change detection is applied for further improvement of the resulting glacier/debris map. A significant percentage of the processing can be done automatically. In order to test the sensitivity of our method against different DEM qualities, it was also applied to a DEM obtained from ASTER stereo data. Additionally, we compared our multisource approach to an artificial neural network (ANN) classification of debris, using only multispectral data. While the combination with an ASTER-derived DEM revealed promising results, the ANN classification without DEM data does not.

Keywords: Glacier mapping; Debris cover; Multispectral classification; DEM analysis

1. Introduction

Changes of mountain glaciers are among the best natural indicators of ongoing climate change (Haeberli et al., 1999; IPCC, 2001; Oerlemans, 1994). The observation of glacier changes is coordinated by several international programs (Haeberli et al., 2000) including the USGS-led project Global Land Ice Measurements from Space (GLIMS), which aims at a global glacier inventory from sensors Advanced Spaceborne Thermal Emission and Reflection Radiometer (ASTER) and Landsat 7 Enhanced Thematic Mapper plus (ETM+) (Kieffer et al., 2000). A number of accurate methods for automated mapping of clean ice (e.g., free of debris cover) and snow by means of multispectral classification is available, for example from thresholded ratio images with Landsat Thematic Mapper (TM) band 4/TM band 5 (e.g., Paul et al., 2002; Sidjak & Wheate, 1999; Williams & Hall, 1998). However, many valley glaciers are covered to a varying extent by supraglacial debris, which has the same spectral characteristics as the surrounding terrain and, thus, cannot be spectrally discerned from it. As a consequence, previous studies related to quantitative assessments of glacier change (area/length) applied manual delineation of debris-covered glaciers, mostly by on-screen digitizing (e.g., Bayr et al., 1994; Hall et al., 1992; Jacobs et al., 1997; Paul, 2002a,b; Williams et al., 1997). Although manual delineation of debris-covered glacier ice generally produces accurate results, it is very time-consuming and labour intensive for studying a larger number of glaciers.

For this reason, we have developed a semi-automatic method that combines pixel-based multispectral classification (clean ice, vegetation) with digital terrain analysis (slope), neighbourhood relations (debris cover/clean ice), and change detection (glacier change). This approach attempts to combine some of the characteristic features of debris-covered glacier ice, which can be utilized for automatic classification. The method is not restricted to Landsat TM data; other sensors with similar spectral bands will work as well. The digital elevation model (DEM) applied has a 25-m cell size and a high accuracy—absolutely mandatory for studying small Alpine glaciers. However, such high-precision DEMs are not available generally for most regions of the earth and we thus have

* Corresponding author. Tel.: +41-1-635-5175.
E-mail address: fpaul@geo.unizh.ch (F. Paul).

0034-4257/$ - see front matter © 2004 Elsevier Inc. All rights reserved.
doi:10.1016/j.rse.2003.11.007

investigated the suitability of a DEM derived from ASTER stereo data.

In this paper, we first present background information on the characteristics of debris-covered glaciers, including relevant previous research on the topic. This review is followed by a more specific description of our multisource method and the data sources used. In Section 4, we applied our multisource method to an experimental test region, including a discussion of the parameters used and the accuracy obtained. Several conclusions are given at the end of the paper.

2. Debris-covered glaciers

2.1. Background

Our multisource method is applied to the Oberaletschgletscher (23 km^2 in area), Swiss Alps, which is located within the larger test region around Grosser Aletschgletscher (24 km long and 86 km^2 in area), which contains many heavily debris-covered glaciers (Fig. 1). In general, the supraglacial debris originates from the surrounding ice-free rock walls, which are prone to intense weathering (Maisch et al., 1999). The debris is transported by the general down-slope movement of a glacier towards the terminus and is deposited in the glacier forefield. If local surface slope is too high, debris usually slides farther down until a more gentle slope allows accumulation. Two typical examples of debris-covered Alpine glaciers are shown in Fig. 2a and b (Oberaletschgletscher and Langgletscher) in synthetic oblique perspective views. They are created from an Indian Remote Sensing (IRS)-1C pan image and a DEM with 25-m spatial resolution (see Fig. 1 for viewing directions).

Distribution and particle sizes of any supraglacial debris are highly variable, ranging from dust-size particles to house-sized blocks and from a minimal occurrence to complete coverage of a glacier tongue (cf. Fig. 2a and b). Very small particles (e.g., dust and soot) are usually distributed gradually in the ablation area, resulting in a characteristic decrease of surface reflection (e.g., Knap et al., 1999; Koelemeijer et al., 1992). The larger-size fraction (e.g., pebbles and boulders) is often arranged to characteristic medial moraines (cf. Fig. 1). The boundary of a debris-covered glacier tongue can either be formed by a lateral moraine (Fig. 3a, top), bedrock valley walls (Figs. 2a and 3a, bottom), or a combination thereof (cf. Fig. 2b). The outer side of a lateral moraine approximates a V-shaped elevation profile (cf. Fig. 3a, top), which may be reproduced by an accurate high-resolution DEM.

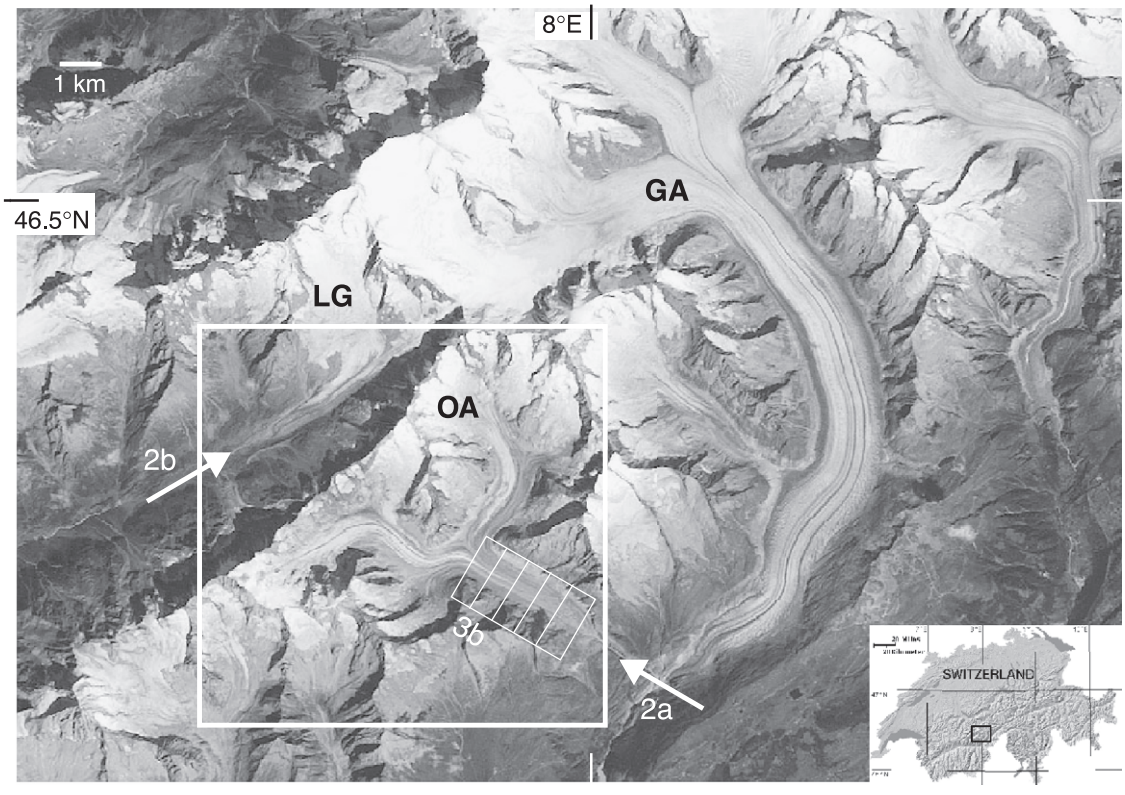

Fig. 1. Location map of the test area (inset) and Landsat TM band 3 image after contrast stretch has been applied. The size of the area is 25 by 17.5 km and includes many debris-covered glaciers (GA = Grosser Aletschgletscher, OA = Oberaletschgletscher, LG = Langgletscher). Also indicated are the viewing directions for Fig. 2a and b (arrows), location and perimeter of transects for Fig. 3b as well as the subsection used for Figs. 4–6 and 8 (box). Landsat TM data: © Eurimage/National Point of Contact (NPOC).

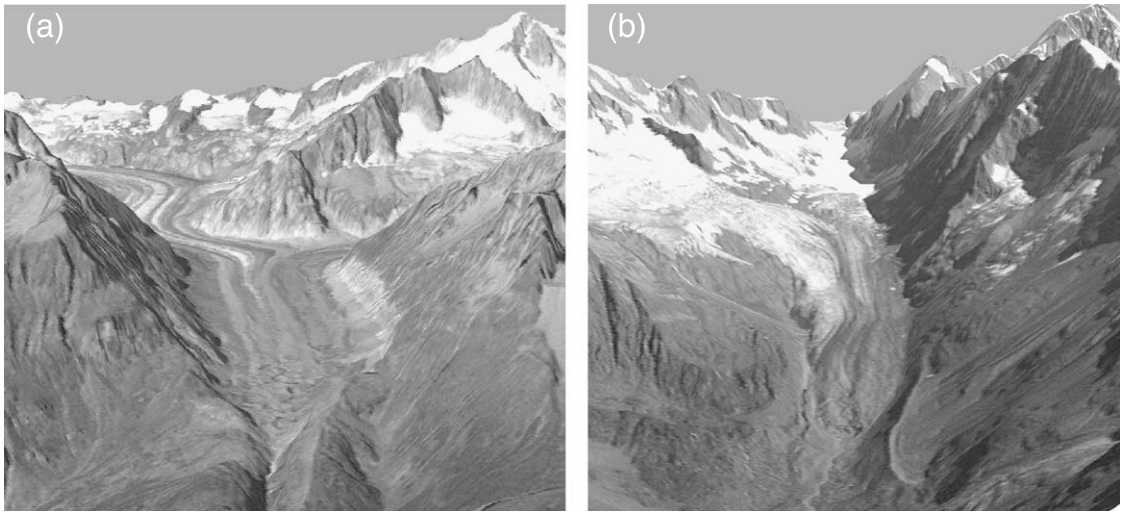

Fig. 2. Synthetic oblique perspective views of: (a) Oberaletschgletscher and (b) Langgletscher generated from a contrast enhanced IRS-1C pan image, which is draped over a DEM. DEM25: © 2003 swisstopo (BA 035782).

Because of the high spatial heterogeneity of the debris-cover, many mixed pixels (ice/debris) occur in optical satellite imagery. If the spectral signal within such a pixel is dominated by the debris, the ice cannot be detected by multispectral classification. Manual delineation is in general still possible, because the glacier boundary exhibits differences in illumination caused by its shape. However, sometimes even in-situ observation is not able to delineate the boundary between supra- and periglacial debris or stagnant ice, and geophysical field investigations might be necessary to detect potential buried glacier ice (Haeberli & Epifani, 1986). Hence, multispectral classification alone is not able to distinguish debris-covered glacier ice from the adjacent periglacial debris.

2.2. Previous works

Earlier studies about mapping of debris-covered glaciers used multispectral classification or geomorphometric DEM analysis alone. Bishop et al. (1995) and Bishop et al. (1999) applied an ANN to estimate the supraglacial debris loads of Himalayan glaciers, using pre-defined glacier outlines. Lougeay (1974) proposed to detect debris that is cooled by underlaying ice by its lower radiometric temperature. This idea was investigated by Taschner and Ranzi (2002) for the Belvedere glacier (Italian Alps); however, they found such a lower temperature only in crevassed regions with partial debris cover. Geomorphometric DEM analysis was applied by Kieffer et al. (2000) to obtain slope and curvature

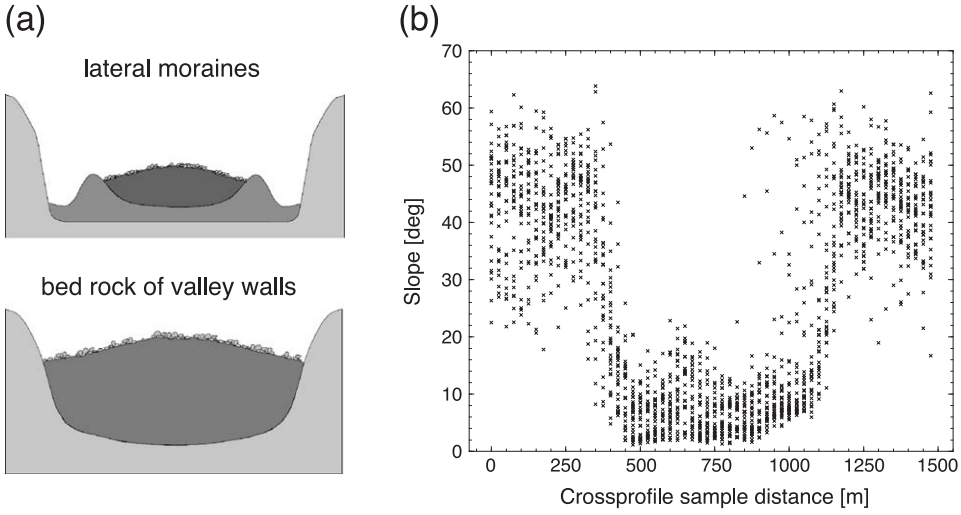

Fig. 3. (a) Schematic cross-sections of typical debris-covered glaciers, top: bounded by lateral moraines, bottom: glacier bounded by bedrock of valley walls. (b) Scatter plot of all slope profiles from 30 transects taken perpendicular to the flow direction and sampled at the lower 2 km of the Oberaletschgletscher tongue from the DEM25 (cf. Fig. 1). In this case, slope values $<20°$ are indicative of the flat debris-covered glacier tongue. DEM25: © 2003 swisstopo (BA 035782).

information. At the contact of the glacier ice with the lateral moraine, a distinct change in curvature was observed, which was utilized in combination with a central flow line for a section-wise delineation of the glacier tongue. Bishop et al. (2000) used flow paths generated by hydrologic modelling from seed points and a V-shaped operator along the outer side of the lateral moraine (cf. Figs. 2b and 3a, top). As such flow lines converge at the glacier snout, they resemble closely the glacier perimeter. The DEM used was obtained photogrammetrically from Systèm Probateire pour l'Observation de la Terre (SPOT) pan stereo imagery for their test site in the Himalaya. Detailed geomorphometric DEM analysis is performed by Bishop et al. (2001) for identification of debris-covered glacier surfaces from so called terrain-form objects.

However, the DEM-based methods discussed above require intense user interaction by specialists; in addition, the task of accurately determining glacier area from the generated outlines or terrain-form objects is not a trivial one. Furthermore, lateral moraines are not that prominent and much smaller in the Alps (Fig. 2b) than in the Himalaya. In the case of rock-wall-restricted glacier beds (cf. Figs. 2a and 3a, bottom), the typical change in curvature along the glacier perimeter might be inconclusive.

3. Methods and data

3.1. Description of methods applied

The previous work discussed above has shown the potential of multispectral classification and DEM analysis for mapping of debris-covered glaciers. However, the methods were not used in combination for mapping of debris-covered glacier ice. In our approach, we combine the advantages of multispectral remote sensing (mapping of clean ice and vegetation free regions) with a DEM-derived slope facet (0–24°). This slope range is not exceeded for most debris-covered glacier tongues, as empirical tests with transects of slope for the lower part of various glacier tongues have shown (e.g., Oberaletschgletscher in Fig. 3b). Most of the vegetation-free and ice-free, steep mountain flanks can be excluded by this combination. However, if their slope is less than 24°, they will remain. As the debris-covered glacier ice has to be contiguous with clean glacier ice, we perform a neighbourhood-analysis to exclude all remaining areas that are not connected to clean glacier ice. In a last step, glacier fluctuations are utilized to detach flat and vegetation-free glacier forefields by means of multitemporal change-detection analysis from sequential images. For debris-covered glaciers without any change at the terminus, as well as for remaining artefacts, final manual editing is applied. The individual steps of this multisource approach are discussed in Section 4 in more detail.

In order to evaluate one of the most advanced methods for pixel-based multispectral classification, we also investigated the suitability of an artificial neural network (ANN) for debris classification (e.g., Bischof et al., 1992; Civco, 1993). We did not test the ANN classification together with DEM data, although ANNs were successfully applied to landcover classification with multisource data, including DEM derivatives (Gong, 1996; Peddle et al., 1994). We used a feed-forward back-propagation network (Pao, 1989) with different network structures tested and empirically evaluated. Best classification results are found for a network with two hidden layers, each with 15 nodes. Determination of the learning rate and momentum rate is based on empirical tests as well as findings from other studies (Haykin, 1998). The network allowed convergence with a learning rate of 0.01 and a momentum rate of 0.9 (system error tolerance = 0.025). Training time could thus be minimized to only 198 iterations.

In view of a possible global application, we also tested a slope facet map obtained from an ASTER-derived DEM in our multisource approach. The DEM was obtained from a 24 August 2001 ASTER scene using 3N and 3B near-infrared stereo bands and standard software (PCI Orthoengine). Apart from major elevation differences on northern slopes (often obstructed by E–W oriented mountain crests), ASTER-derived DEMs may provide sufficient accuracy for mapping of gently sloping debris-covered glacier tongues (Kääb, 2002).

3.2. Data sources

We applied our combined analytical approach with TM data from 31 August 1998 (and 12 September 1985), and the DEM25 from the Swiss Federal Office of Topography (Swisstopo, 2001). However, the multispectral classification of clean glacier ice/snow and vegetation only requires a red, near infrared (NIR) and middle-infrared (MIR) band (i.e., TM bands 3, 4, and 5), which are also available from numerous other sensors (e.g., ASTER, IRS-1C/D, SPOT 4/5). Besides its high-spatial resolution (25 m), the DEM25 also has a high vertical accuracy (a few meters) that is rarely available for most parts of the world. However, globally available ASTER-derived DEMs or future Shuttle Radar Topography Mission (SRTM)-derived products are probably sufficient for debris-cover mapping of the much larger glaciers elsewhere in the world (e.g., Alaska, Himalaya, Andes).

4. Results and discussion

4.1. The multisource method

In this section, we describe the individual steps used in our multisource, debris-cover mapping approach and follow with a discussion of the threshold values applied. The steps are illustrated in Figs. 4–6 for the subregion Oberaletschgletscher (see white box in Fig. 1), and the processing workflow is drawn schematically in Fig. 7. Results from the multispectral ANN classification and the use of the

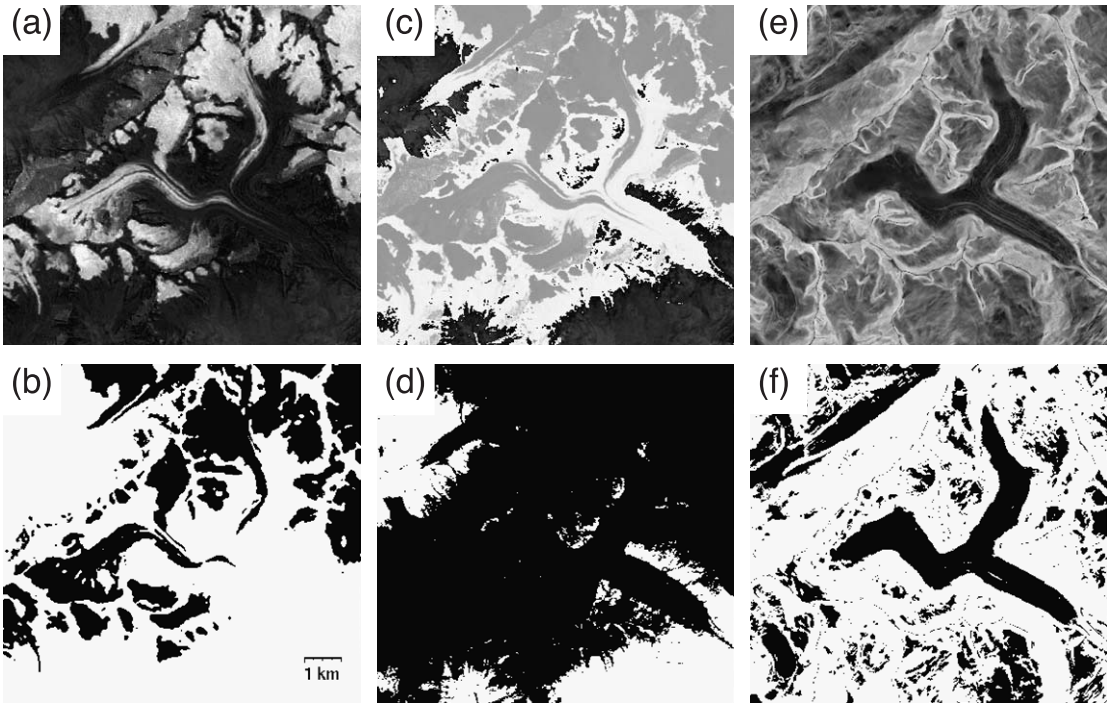

Fig. 4. Selected processing steps for illustration of the debris-cover mapping algorithm. (a) TM4/TM5 ratio image, (b) resulting glacier map after thresholding, (c) hue-component from intensity hue saturation colour space transformation, (d) resulting map of vegetation free areas (black) after thresholding, (e) slope as derived from the DEM25, and (f) slope facet, showing all slopes $<24°$ in black. DEM25 © 2003 swisstopo (BA 035782).

multisource method with an ASTER-derived DEM are discussed afterwards. The processing steps are as follows:

(1) A TM4/TM5 band-ratio image (Fig. 4a) is segmented into the classes 'glacier' (black) and 'other' (white) using a threshold value of 2.0 (Fig. 4b).
(2) The hue-component of an intensity hue saturation (IHS)-colour-space transformation from TM bands 3, 4, and 5 (Fig. 4c) is used to map vegetation (white) and vegetation-free areas (black) with a threshold value of 126 (Fig. 4d). The vegetation map is also used to reduce misclassification of pixels during glacier mapping. In pseudo code, the glacier classification is (pix = 0 means 'glacier'):

IF ((TM4/TM5) > 2.0) AND (hue345 > 126)
THEN pix = 0 else pix = 255.

(3) Slope is calculated from the DEM25 (Fig. 4e) and all slope values $<24°$ are used for the slope facet map (black in Fig. 4f).

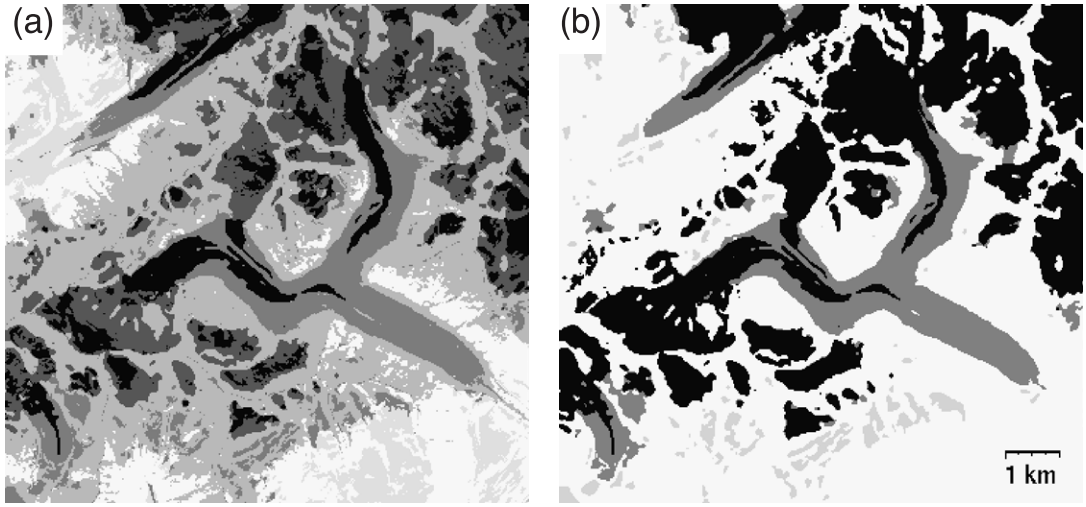

Fig. 5. (a) Overlay of the binary glacier, vegetation, and slope maps (Fig. 4b, d, and f). The legend for the grey shades is given in Table 1. (b) The resulting classes glacier (black), debris (grey), and debris, which is not connected to a glacier (light grey).

Table 1
Legend to the grey levels used in Fig. 5a (–=no, x=yes)

	White	Light grey	Grey	Dark grey	Very dark grey	Black
Slope < 24° ?	-	X	-	X	-	X
Vegetation ?	X	X	-	-	-	-
Glacier ?	-	-	-	-	X	X
Classification		other		debris	glacier	

The final classification is summarized in the last row.

(4) The overlay of all three black-and-white maps is presented in Fig. 5a in shades of grey with the legend given in Table 1. The class 'debris' is produced from the pseudo code (pix = 255 means 'no glacier', pix = 127 means 'debris'):

IF (pix = 255) AND (hue345 > 126) AND (slope < 24)
THEN pix = 127.

In order to reduce misclassification of pixels and noise, a 3 by 3 median filter is applied after the classification. The result is shown in Fig. 5b (glacier = black, debris = grey), also depicting areas with 'debris' that are not connected to glaciers (light grey). They are marked by the 'image polygon growing' (IPG) module from the digital image processing software PCI (1998).

(5) With IPG, individual numbers (ID) are assigned to all areas that are connected (8-point connectivity) to the class 'glacier' or 'debris'. These numbers are written to a text file for each pixel together with their respective grey values (0 or 255) from the classified glacier map. A Fortran program seeks for debris IDs without corresponding glacier IDs, thus removing isolated 'debris' regions from the map (light grey in Fig. 5b).

(6) For the multitemporal change-detection map, the raw data from TM5 of 1998 are subtracted from those in 1985, resulting in a black seam where a change from 'dark' glacier pixels to 'bright' debris pixels took place (Fig. 6a). This map is converted to a binary-change map by segmentation (Fig. 6b) and combined with Fig. 5b to indicate regions of glacier change.

The threshold used for glacier mapping from TM4/TM5 band-ratio images is, in general, quite robust, but should be verified by visual inspection (Paul et al., 2002). In particular, glaciers in shadow areas are sensitive to the threshold value. The lower the threshold, the more of the partly debris-covered pixels are included, but at the expense of more noise elsewhere. Mapping of vegetated areas is also possible from the NDVI, but at the cost of additional processing, such as data adjustments (cf. Crippen, 1988) and threshold selection. The use of a higher threshold value for the slope facet may include larger parts of steeper, debris-covered glaciers, but will lead to more connected forefield regions elsewhere. The slope threshold selected (i.e. < 24°) is based on empirically tested values and adjusted to minimize the remaining manual corrections.

TM5 is used for the glacier-change map, because shadowed areas have a similar low reflectance as glaciers in the MIR-band, and differences caused by changed illumination conditions are thus less visible. The difference between two scenes is superior to their ratio, because small differences in digital numbers within glaciers are less pronounced. The map produced from change detection is also used to update the glacier outlines with respect to the acquisition date of the DEM. Manual editing by changing colours of detached regions to 'background' and correction of remaining artefacts (e.g., where slope of debris-covered glacier ice >24°) is applied as the final step (cf. Fig. 7). We found that a TM band 5, 4, and 3 composite, with an overlay of the automatically derived glacier areas, is best suited for this final manual editing.

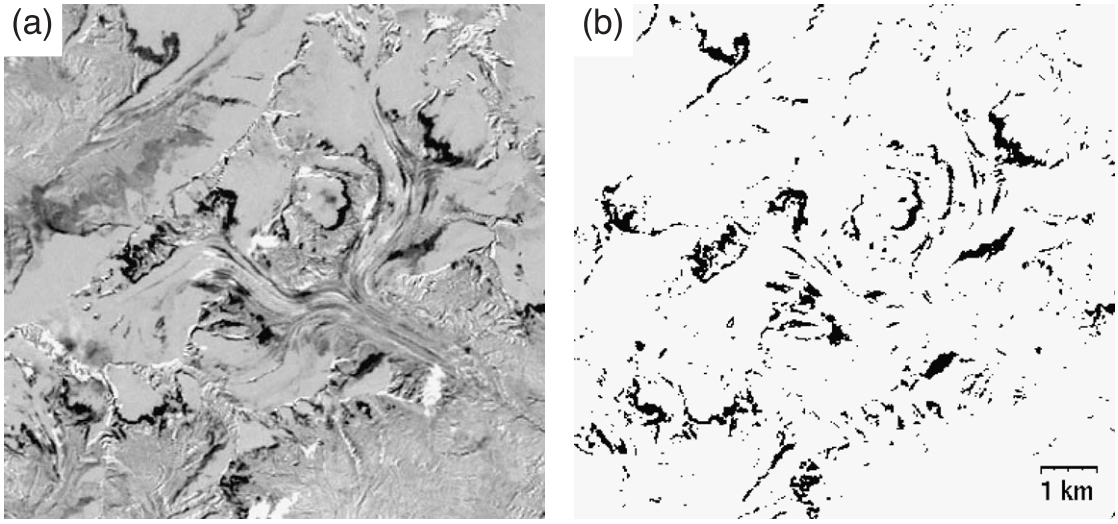

Fig. 6. Multitemporal image analysis: (a) TM5 (1985) – TM5 (1998) after contrast stretching. Regions, which are subject to change, appear black or white. (b) After segmentation, most of the black pixels indicate change due to glacier fluctuations.

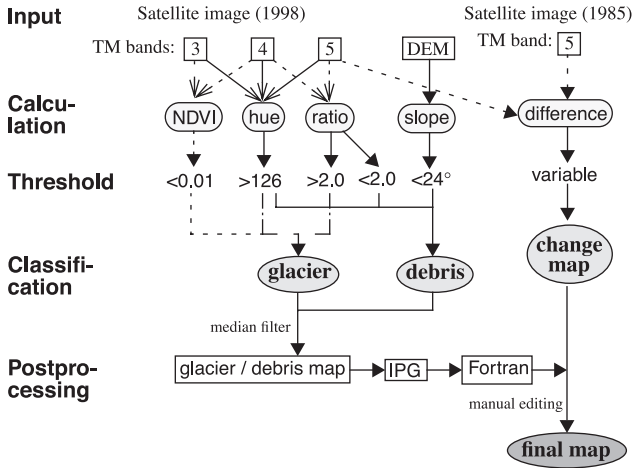

Fig. 7. Schematic workflow for debris-covered glacier mapping. The first row marks the input (TM bands or DEM) required for calculation of the products mentioned in the second row. The normalized difference vegetation index (NDVI) is added as an alternative to the hue-component. The third row gives the threshold parameters used and the forth row the maps generated. The 'post-processing' row summarizes the final editing.

Our method adds 6% of debris-covered ice to the 34% of clean ice within the test region (cf. Fig. 1), which corresponds to a 17% increase in glacier area. Final editing deletes 21% of the previously assigned debris cover, which is 2.5% of the total glacier area. A verification of the accuracy is presented in Fig. 8a by comparison with a vector data set from 1993 ('debris on glacier ice'), which has been created by the Swiss Federal Office of Topography. The good correspondence (partially edge sharp) is obvious, although some deviations exist (see arrows) where: (a) slope >24° and (b) glacier recession since 1993 did occur. Deviations of type (a) can be corrected during final manual editing.

4.2. The ANN classification

In view of the possible application in remote and high-mountain regions with poor reference data, the use of a relatively small training set was specifically intended (Hepner et al., 1990). Five classes are defined: debris, bare ice, rock, vegetation, and shadowed areas. No distinction is made between debris cover on glaciers and other debris within the test area. Though this does not meet completely the objective of mapping debris-covered glaciers, it is still very valuable to evaluate the performance of an ANN in mapping unconsolidated debris.

The classification results for the class 'debris' are compared to ground-truth data obtained from visual interpretation of the TM scene and topographic maps. The overall accuracy was 0.64 with a kappa coefficient of 0.26, what is not satisfactory (Congalton, 1991). In comparison with the independent vector debris layer (cf. Fig. 8a), the overall accuracy is 0.75 and the kappa coefficient is 0.22. As can be seen in Fig. 8b, the amount of correctly classified debris-cover pixels (dark grey) is much higher on Langgletscher than on Oberaletschgletscher (cf. Fig. 1). Most misclassifications of pixels (light grey and black) are related to bedrock areas because their spectral signature is very similar to that of debris. Thus, the performance of the ANN classifier for mapping debris is not convincing as the accuracy measures showed.

4.3. The ASTER DEM

In Fig. 9, the debris-cover classification based on the slope facet from the ASTER DEM is compared to the DEM25 classification for a part of the total test region (cf. Fig. 1). Apart from an overall good correspondence, many

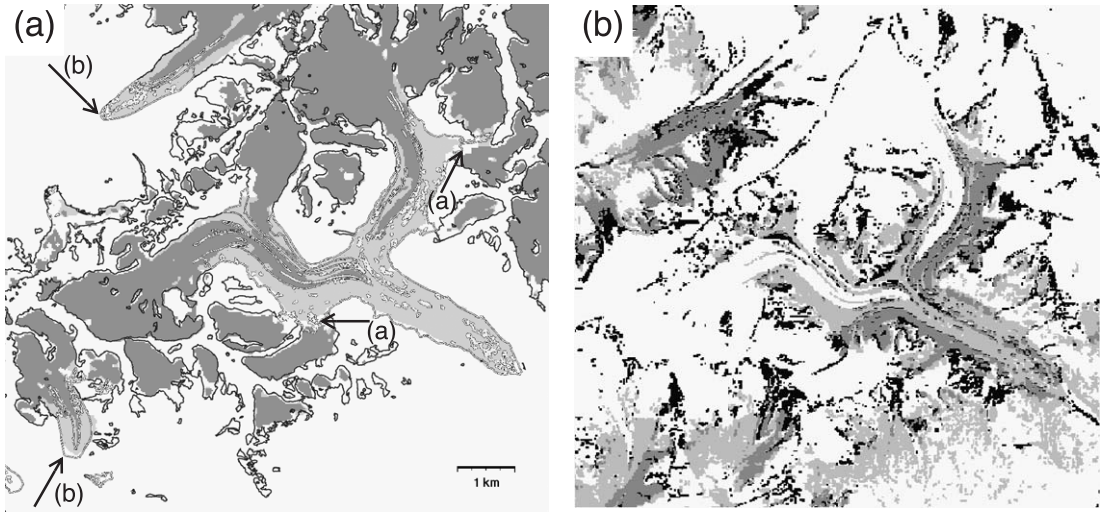

Fig. 8. (a) Comparison of the classified image (dark grey = glacier, light grey = debris) with outlines from the vector data set (black = glacier, white with black border = debris on glaciers). Arrows indicate differences discussed in the text. (b) ANN classification of debris compared to ground truth. Grey shades denote: dark grey = correctly classified pixels, light grey = debris cover only in the ground truth, black = debris cover only in the ANN classification.

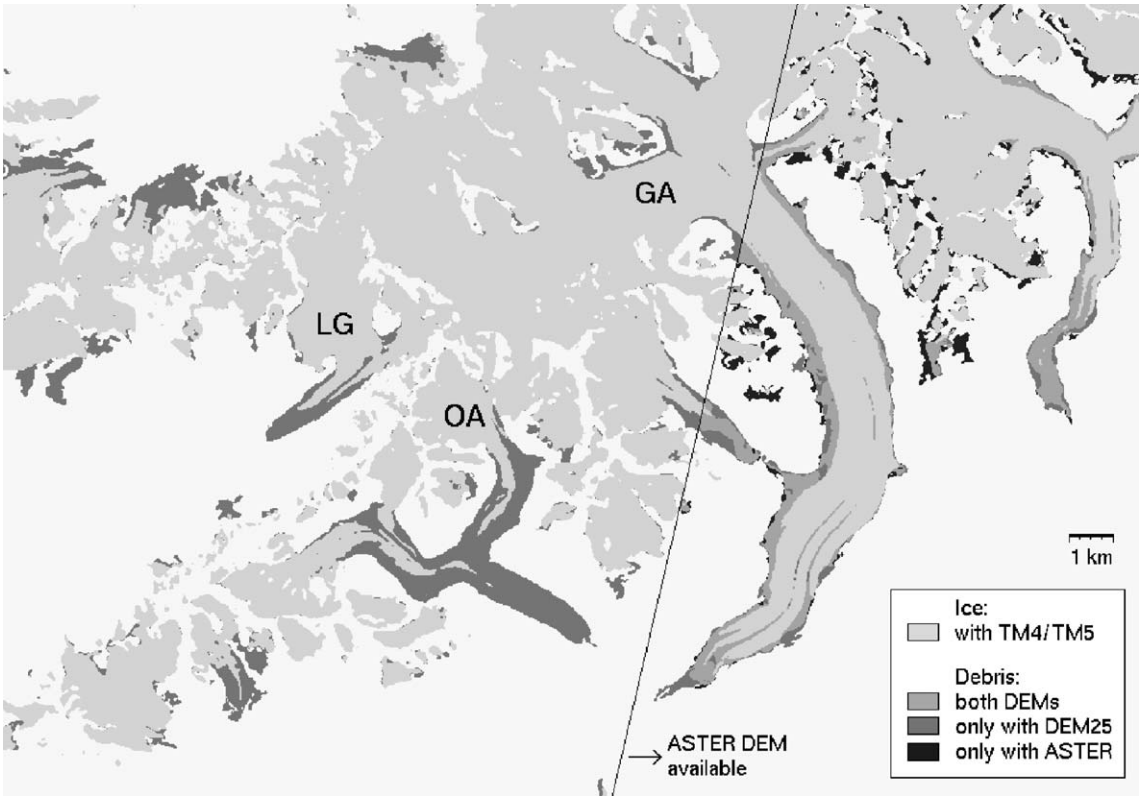

Fig. 9. Comparison of the debris classification for the entire test region using the DEM25 and the ASTER-derived DEM. Clean glacier ice is light grey, debris mapped from both DEMs is grey, debris mapped only from the DEM25 is dark grey, and debris mapped only from the ASTER DEM is black. DEM25: © 2003 swisstopo (BA 035782).

deviations are also visible. In particular, artefacts of the ASTER DEM increase the number of erroneously classified regions, mainly at W-E oriented mountain crests, which may obstruct terrain in the back-looking band 3B (e.g., Kääb et al., 2003). Additional correction of such DEM errors prior to slope calculation may reduce such artefacts and improve the classification. However, DEMs derived from ASTER stereo data may provide useful results for many remote high-mountain regions with poor or inaccessible DEM data.

5. Conclusions

Future remote sensing based glacier inventorying will have to consider supraglacial debris as a common feature at the surface of a glacier in the ablation area. Such debris-covered glacier ice has been widely recognized as the main obstacle for automatic glacier mapping. We have presented a semi-automatic method for delineation of debris-covered glaciers, which combines multispectral image classification (glacier ice, vegetation) with DEM data (slope), neighbourhood analysis (connection to glacier ice), and change detection. The advantage of this multisource approach is the automatic processing, which is based on simple rules, as well as the pixel-based classification of the debris-covered region itself. With an appropriate DEM, accurate orthorectification and some final editing, the accuracy obtained can be equal to pixel resolution. For a large number of glaciers (hundreds), the method is much faster than manual delineation alone, even if the final manual editing is considered. For manual delineation of a few glaciers, the resulting debris-cover map is an efficient starting point nevertheless.

The results from the ANN classification of debris-cover based on multispectral properties alone are not satisfactory. However, integration of slope data in ANN classification may improve results considerably, because multisource data classification with ANNs by other authors offer promising results (e.g., Peddle et al., 1994).

Because of the initial errors of ASTER-derived DEMs for steep, high-mountain relief, the derived slope facet show such artefacts as well. However, for the gentle slopes of debris-covered glacier tongues, the ASTER DEM has a great potential to facilitate glacier mapping from a global perspective.

Acknowledgements

We would like to thank R. Williams for his careful and constructive review. This study has been made possible by two grants from the Swiss National Science Foundation (contracts 21-54073.98 and 21-59045.99).

References

Bayr, K. J., Hall, D. K., & Kovalick, W. M. (1994). Observations on glaciers in the eastern Austrian Alps using satellite data. *International Journal of Remote Sensing*, *15*, 1733–1742.

Bischof, H., Schneider, W., & Pinz, A. J. (1992). Multispectral classification of Landsat-images using neural networks. *IEEE Transactions on Geoscience and Remote Sensing*, *30*(3), 482–490.

Bishop, M. P., Bonk, R., Kamp, U., & Shroder Jr., J. F. (2001). Terrain analysis and data modeling for alpine glacier mapping. *Polar Geography*, *25*(3), 182–201.

Bishop, M. P., Kargel, J. S., Kieffer, H. H., MacKinnon, D. J., Raup, B. H., & Shroder Jr., J. F. (2000). Remote-sensing science and technology for studying glacier processes in high Asia. *Annals of Glaciology*, *31*, 164–170.

Bishop, M. P., Shroder Jr., J. F., & Hickman, B. L. (1999). SPOT panchromatic imagery and neural networks for information extraction in a complex mountain environment. *Geocarto International*, *14*, 19–28.

Bishop, M. P., Shroder Jr., J. F., & Ward, L. J. (1995). SPOT multispectral analysis for producing supraglacial debris-load estimates for Batura Glacier, Pakistan. *Geocarto International*, *10*, 81–90.

Civco, D. L. (1993). Artificial neural networks for land-cover classification and mapping. *International Journal of Remote Sensing*, *7*(2), 173–186.

Congalton, R. G. (1991). A review of assessing the accuracy of classifications of remotely sensed data. *Remote Sensing of Environment*, *37*, 35–46.

Crippen, R. E. (1988). The dangers of underestimating the importance of data adjustments in band ratioing. *International Journal of Remote Sensing*, *9*, 767–776.

Gong, P. (1996). Integrated analysis of spatial data from multiple sources: Using evidential reasoning and an artificial neural network for geological mapping. *Photogrammetric Engineering and Remote Sensing*, *62*(5), 513–523.

Haeberli, W., & Epifani, F. (1986). Mapping the distribution of buried glacier ice—an example from Lago delle Locce, Monte Rosa, Italian Alps. *Annals of Glaciology*, *8*, 241–246.

Haeberli, W., Cihlar, J., & Barry, R. (2000). Glacier monitoring within the global climate observing system. *Annals of Glaciology*, *31*, 241–246.

Haeberli, W., Frauenfelder, R., Hoelzle, M., & Maisch, M. (1999). Rates and acceleration trends of global glacier mass changes. *Geografiska Annaler*, *81A*, 585–591.

Hall, D. K., Williams Jr., R. S., & Bayr, K. J. (1992). Glacier recession in Iceland and Austria, EOS, *Transactions, American Geophysical Union, 73*(12).

Haykin, S. (1998). *Neural networks, a comprehensive foundation*. Prentice Hall, New Jersey, 842 pp.

Hepner, G. F., Logan, T., Ritter, N., & Bryant, N. (1990). Artificial neural network classification using a minimal training set: Comparison to conventional supervised classification. *Photogrammetric Engineering and Remote Sensing*, *56*(5), 469–473.

IPCC (2001). In J. T. Houghton, Y. Ding, D. J. Griggs, M. Noguer, P. J. van der Linden, & D. Xiaosu (Eds.), *Climate Change 2001: The scientific basis. Contribution of working group I to the third assessment report*. Cambridge Univ. Press, Cambridge, UK, 944 pp.

Jacobs, J. D., Simms, E. L., & Simms, A. (1997). Recession of the southern part of Barnes Ice Cap, Baffin Island, Canada, between 1961 and 1993, determined from digital mapping of Landsat TM. *Journal of Glaciology*, *43*(143), 98–102.

Kääb, A. (2002). Monitoring high-mountain terrain deformation from repeated air- and spaceborne optical data: Examples using digital aerial imagery and ASTER data. *ISPRS Journal of Photogrammetry and Remote Sensing*, *57*, 39–52.

Kääb, A., Paul, F., Huggel, C., Kieffer, H., Kargel, J., & Wessels, R. (2003). Glacier monitoring from ASTER imagery: Accuracy and applications. *EARSeL workshop on remote sensing of land ice and snow, Berne, 11.-13.3.2002. EARSeL eProceedings, 2*, 43–53 (CD-ROM).

Kieffer, H., et al. (2000). New eyes in the sky measure glaciers and ice sheets. *EOS, Transactions, American Geophysical Union*, *81*(24), 265, 270, 271.

Knap, W. H., Brock, B. W., Oerlemans, J., & Willis, I. C. (1999). Comparison of Landsat-TM derived and ground-based albedo of Haut Glacier d'Arolla. *International Journal of Remote Sensing*, *20*(17), 3293–3310.

Koelemeijer, R., Oerlemans, J., & Tjemkes, S. (1992). The surface reflectance of the Hintereisferner from Landsat 5 TM imagery. *Annals of Glaciology*, *17*, 17–22.

Lougeay, R. (1974). Detection of buried glacial and ground ice with thermal infrared remote sensing. In H. S. Santeford, & J. L. Smith (Eds.), *Advanced concepts and techniques in the study of snow and ice resources* (pp. 487–494). Washington, DC: National Academy of Sciences.

Maisch, M., Haeberli, W., Hoelzle, M., & Wenzel, J. (1999). Occurrence of rocky and sedimentary glacier beds in the Swiss Alps as estimated from glacier-inventory data. *Annals of Glaciology*, *28*, 231–235.

Oerlemans, J. (1994). Quantifying global warming from the retreat of glaciers. *Science*, *264*, 243–245.

Pao, Y. H. (1989). *Adaptive pattern recognition and neural networks*. Massachusetts: Addison-Wesley Publishing (309 pp.).

Paul, F. (2002a). Combined technologies allow rapid analysis of glacier changes. *EOS, Transactions, American Geophysical Union*, *83*(23), 253, 260, 261.

Paul, F. (2002b). Changes in glacier area in Tyrol, Austria, between 1969 and 1992 derived from Landsat 5 TM and Austrian Glacier Inventory data. *International Journal of Remote Sensing*, *23*(4), 787–799.

Paul, F., Kääb, A., Maisch, M., Kellenberger, T., & Haeberli, W. (2002). The new remote sensing derived Swiss glacier inventory. I: Methods. *Annals of Glaciology*, *34*, 355–361.

PCI (1998). *Software package for digital image processing, version 6.3. © PCI*. Richmond Hill, Ontario, Canada.

Peddle, D. R., Foody, G. M., Zhang, A., Franklin, S. E., & LeDrew, E. F. (1994). Multi-source image classification. II: An empirical comparison of evidential reasoning and neural network approaches. *Canadian Journal of Remote Sensing*, *20*(4), 396–407.

Sidjak, R. W., & Wheate, R. D. (1999). Glacier mapping of the Illecillewaet Icefield, British Columbia, Canada, using Landsat TM and digital elevation data. *International Journal of Remote Sensing*, *20*(2), 273–284.

Swisstopo (2001). *DHM25-Das digitale Höhenmodell der Schweiz Level 2* (pp. 1–17). Bundesamt für Landestopographie, Wabern (URL: http://www.swisstopo.ch/de/digital/dhm25.htm, access: 10 November 2003).

Taschner, S., & Ranzi, R. (2002). Landsat-TM and ASTER data for monitoring a debris covered glacier in the Italian Alps within the GLIMS project. *Proceedings IGARSS 2002*, *4*, 1044–1046.

Williams Jr., R. S., & Hall, D. K. (1998). Use of remote-sensing techniques. In W. Haeberli, M. Hoelzle, & S. Suter (Eds.), *Into the second century of worldwide glacier monitoring: Prospects and strategies* (pp. 97–111). Paris: UNESCO Publishing.

Williams Jr., R. S., Hall, D. K., Sigurdsson, O., & Chien, J. Y. L. (1997). Comparison of satellite-derived with ground-based measurements of the fluctuations of the margins of Vatnajökull, Iceland, 1973–1992. *Annals of Glaciology*, *24*, 72–80.